Nanoscale

PAPER

View Article Online
View Journal | View Issue



Cite this: *Nanoscale*, 2015, **7**, 20220

# The effect of nanocrystalline silicon host on magnetic properties of encapsulated iron oxide nanoparticles†

P. Granitzer,*[a] K. Rumpf,[a] R. Gonzalez-Rodriguez,[b] J. L. Coffer[b] and M. Reissner[c]

Received 3rd August 2015,
Accepted 12th November 2015

DOI: 10.1039/c5nr05232g

www.rsc.org/nanoscale

The purpose of this work is a detailed comparison of the fundamental magnetic properties of nanocomposite systems consisting of $Fe_3O_4$ nanoparticle-loaded porous silicon as well as silicon nanotubes. Such composite structures are of potential merit in the area of magnetically guided drug delivery. For magnetic systems to be utilized in biomedical applications, there are certain magnetic properties that must be fulfilled. Therefore magnetic properties of embedded $Fe_3O_4$-nanoparticles in these nanostructured silicon host matrices, porous silicon and silicon nanotubes, are investigated. Temperature-dependent magnetic investigations have been carried out for four types of iron oxide particle sizes (4, 5, 8 and 10 nm). The silicon host, in interplay with the iron oxide nanoparticle size, plays a sensitive role. It is shown that $Fe_3O_4$ loaded porous silicon and SiNTs differ significantly in their magnetic behavior, especially the transition between superparamagnetic behavior and blocked state, due to host morphology-dependent magnetic interactions. Importantly, it is found that all investigated samples meet the magnetic precondition of possible biomedical applications of exhibiting a negligible magnetic remanence at room temperature.

## Introduction

Nanostructured semiconductors are of interest in multiple fields such as optics,[1] chemical[2] and biological sensing[3] as well as biomedicine.[4] One type of nanostructured semiconductor is porous silicon (pSi), which offers high surface areas,[5] a broadly-tunable morphology,[6] a porosity-dependent resorption behavior *in vivo*,[7] and the ability to act as a host material for a multitude of different materials and molecules.[8,9] In particular, the combination of porous silicon with magnetic nanostructures offers advantages by the integration of device-relevant magnetic nanoscopic systems with biocompatible,[10] biomedically-relevant pSi structures. In terms of possible magnetic nanostructure candidates, superparamagnetic iron oxide nanoparticles (NPs) are of widespread interest in current biomedical research for both diagnostics and therapy;[11] examples include hyperthermia,[12] magnetic resonance imaging[13] and gene delivery.[14] While the fundamental magnetic properties of iron oxide nanoparticles, especially of the magnetite ($Fe_3O_4$) phase, have been extensively investigated,[15] their use in conjunction with high surface area porous matrices offers the opportunity to pack a relatively high density of such magnetic nanoparticles in a small volume and evaluate possible changes in magnetic interactions between them. In principle, strategies that increase concentration of these magnetic nanostructures could facilitate their use as targeting vehicles *in vivo*.

pSi has been greatly investigated for relevance in both therapeutic applications and biosensing,[7–16] but there are nevertheless challenges associated with achieving desired monodispersity of the porous silicon particles, which are often size selected by ball milling.[17] To overcome this drawback, silicon nanotubes (SiNTs) of a clearly-defined size and a uniform structure have been explored as an alternative. The length, along with the outer and inner diameter of the SiNTs, are in principle broadly tunable, with a wall thickness-dependent aqueous dissolution behavior.[18] In the specific studies reported here, SiNTs of ~2 μm in length, a well-defined cylindrical cavity and inner diameter of ~50 nm, and average wall thicknesses of 10 and 70 nm have been used. Structures with

[a]*Institute of Physics, Karl-Franzens-University Graz, 8010 Graz, Austria. E-mail: petra.granitzer@uni-graz.at*
[b]*Department of Chemistry, Texas Christian University, Fort Worth, TX, USA*
[c]*Institute of Solid State Physics, Vienna University of Technology, 1040 Vienna, Austria*

†Electronic supplementary information (ESI) available: Energy dispersive X-ray spectra and corresponding EDX maps of pSi filled with $Fe_3O_4$-NPs of 8 nm and of 5 nm are shown. Furthermore the process for loading $Fe_3O_4$ NPs into Si NTs, consisting of: (a) physical detachment of SiNTs grown on a substrate and inversion of the NT film, followed by (b) dropwise addition of a solution of $Fe_3O_4$ NPs, facilitated by placing a Nd magnet underneath the film; (c) subsequent formation of the $Fe_3O_4$ NP-loaded SiNTs is depicted. The size dependent blocking temperatures of SiNTs of 10 nm wall thickness filled with $Fe_3O_4$ NPs are summarized in a table. TEM image and associated size distribution data for a commercial $Fe_3O_4$ NP sample (Aldrich) with stated average particle size of 10 nm is also shown. See DOI: 10.1039/c5nr05232g

these dimensions are in principle capable of being engulfed by engaging cells. The values for the SiNTs are selected due to previous studies suggesting a porous silicon particle size range of ~3.5 μm of hemispherical shape for optimal circulatory behavior in plasma.[19] It has been shown that needle-shaped carbon nanotubes offer a toxic behavior[20] and thus it is of importance to use nanomaterials with low toxicity which can biodegrade in a reasonable time or which can be eliminated from or associated with the body in a harmless way. In both of the morphologies evaluated here, nanostructured silicon offers all of these preconditions and thus is an excellent candidate.

## Methods

### Porous silicon

The pSi templates are prepared by anodization of a highly n-doped silicon wafer in an aqueous hydrofluoric acid solution offering average pore-diameters of 60 nm, a mean distance between the pores of 50 nm and an average pore-length of 35 μm. As electrolyte a hydrofluoric acid solution consisting of $HF:C_2H_6O:H_2O$ in the ratio 1 : 1 : 2 was used. A current density of 100 mA $cm^{-2}$ was applied during the anodic etching process. After the etching procedure the samples were aged in air for several days to obtain a native oxide layer. This oxide layer decreases with increasing pore-depth (as evaluated by energy dispersive X-ray (EDX)-spectroscopy). In all pSi templates used here the pores are oriented and clearly separated from each other. Fig. 1a shows a TEM image of a porous silicon sample in cross-section.

The iron oxide NPs have been fabricated using a well-known route involving high temperature decomposition.[21,22] Further details about the fabrication process of the iron oxide nanoparticles can be found in previous publications.[21,22] These templates have been filled with iron oxide nanoparticles of either 4, 5, 8 or 10 nm. In Fig. 1b NPs with a mean diameter of 8 nm can be seen within the pores.

The filling procedure with iron oxide NPs has been performed by adding drops of a given nanoparticle solution onto the sample surface. To facilitate the infiltration process a NdFeB magnet with a pole field strength of 1 T was used.

### Silicon nanotubes

SiNTs are fabricated by a sacrificial template method reported previously by our research group.[18] It involves the initial formation of ZnO nanowire array (NWA) templates on a substrate (such as silicon wafers or F-doped tin oxide (FTO) glass), followed by Si deposition (530 °C for 10 nm shell thickness Si NTs, 580 °C for 70 nm shell thickness), and subsequent template removal by a $NH_3$/HCl etch under a helium atmosphere at 400 °C. ZnO NWA templates were prepared on a given substrate (FTO or Si) that were previously seeded with ZnO nanocrystals (according to a previously-described procedure[18]) by placing in a mixture (1 : 1 v : v) of 0.03 M $Zn(NO_3)_2$ and 0.03 M hexamethylenetetramine at 92 °C for 9 h. Polyethylenimine (100 μl, branched, low molecular weight, Aldrich) was added into 100 ml of ZnO growth solution. A ZnO NWA sample was inserted into a quartz tube reactor and Si deposition on the ZnO NWA was achieved through the use of silane (20 sccm, 0.5% in He) mixed with He carrier gas (200 sccm) that was passed through a furnace operating at 530 °C for 10 nm wall thickness, 540 °C for 40 nm wall thickness and 580 °C for 70 nm wall thickness. These Si-coated ZnO NW samples were then placed in another quartz reactor and heated to 450 °C; $NH_4Cl$ was loaded in an alumina boat located upstream and heated to 350 °C. The gaseous etchant was transported *via* He gas downstream (170 sccm) to the furnace for 1 h for removal of the ZnO NWA template.

While the pSi samples offer a decreasing oxide gradient towards the pore-tips in terms of surface chemistry, the SiNTs offer an uniform native oxide surface layer over their entire length. These nanotubes are filled with the same iron oxide nanoparticles of the different sizes named above (Fig. 2).

In each case, porous silicon as well as the SiNTs, a magnetic field has been applied to facilitate the infiltration process of the particles into the pores/tubes. The loading of 4 nm $Fe_3O_4$ NPs in SiNTs with a 10 nm shell thickness is achieved *via* simple diffusion involving soaking the sample in the $Fe_3O_4$ NPs solution (7 mg $mL^{-1}$, oleic acid terminated, hexane solution) for 2 h. For larger diameter NPs and/or SINTs with

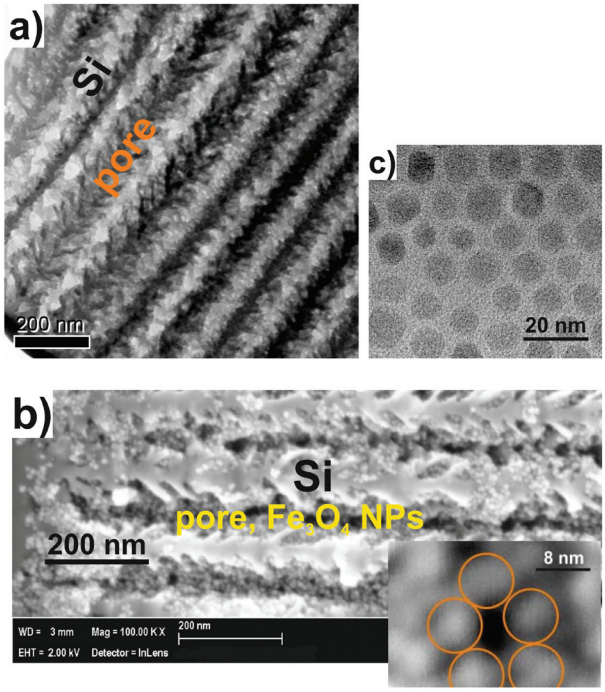


**Fig. 1** (a) cross-sectional TEM image of a typical used porous silicon template showing the pores (average pore diameter 60 nm) and the remaining silicon (mean distance between the pores 50 nm). (b) SEM image in cross-section showing iron oxide NPs of about 8 nm in size within the pores. The inset shows individual NPs of about 8 nm which are arranged within a pore. (c) TEM image of 8 nm $Fe_3O_4$ nanoparticles. The distance between the particles is around 4 nm which is twice the thickness of the coating of 2 nm.

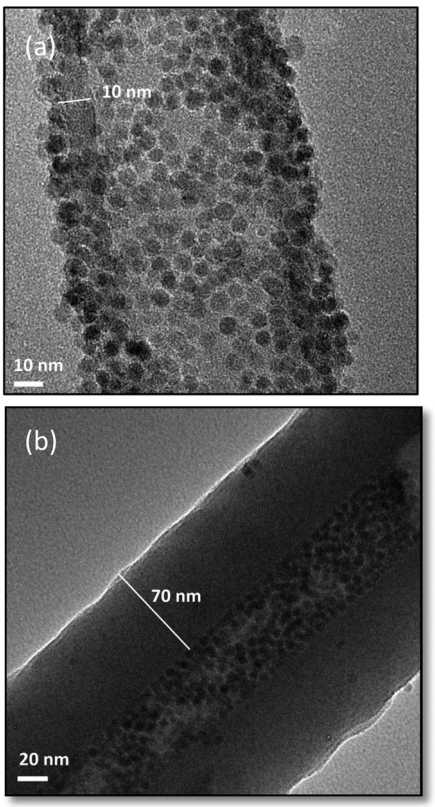


Fig. 2 SiNTs loaded with 4 nm $Fe_3O_4$ NPs: (a) 10 nm shell thickness. (b) 70 nm shell thickness.

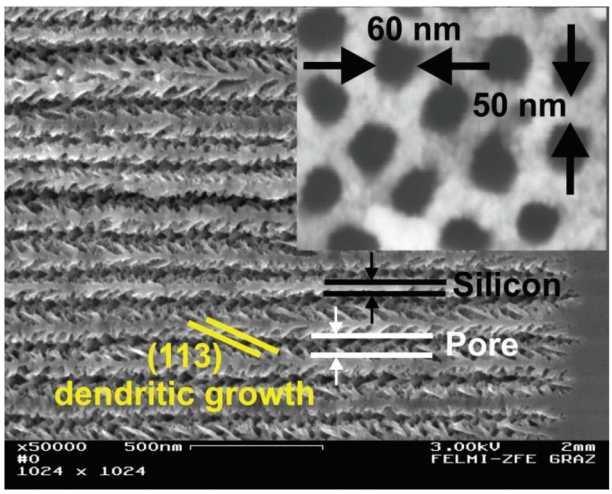


Fig. 3 Cross-sectional SEM image of a typical porous silicon sample showing the dendritic growth of the pores. The main pores grow in (100) direction whereas the dendrites grow in (113) direction with much lower growth rate. In the inset a top view image shows the quite regular pore arrangement with pore diameters of about 60 nm and distances between the pores of about 50 nm.

thicker walls, loading of the SiNTs with $Fe_3O_4$ NPs is readily achieved by initial removal of the SiNT film from the underlying substrate (such as FTO glass) and placing it face down on top of a Nd magnet with a piece of filter paper in between. $Fe_3O_4$ NPs (same concentration noted above) are added dropwise, followed by rinsing the sample with acetone several times, and allowed to air dry.

## Results and discussion

The microstructure of the pSi templates used here offers a dendritic pore morphology with side-pores in the range of 20 nm. The main pores grow in the (100) direction, and the side-pores in the (113) direction.[23] A typical porous silicon morphology is shown in Fig. 3. This results in a reduced effective distance between the pores of about 10 nm.

In contrast, the SiNTs offer a more uniform wall structure, with a separation distance of magnetic NPs between tube interiors that is effectively two times the wall thickness of a given type of SiNT (*i.e.* either 20 nm or 140 nm total distance). These nanotubes also clearly lack the dendritic side pore structure of the pSi films. Due to their size, the infiltrated iron oxide nanoparticles are superparamagnetic and because of the thickness of the organic oleic acid coating of ~2 nm, magnetic exchange interaction is suppressed. Nevertheless, if the particles are closely packed, magnetic dipolar coupling provokes a hysteretic behavior of the magnetization of the nanocomposite below the blocking temperature.

### Magnetic properties

The magnetic properties of the pSi/iron oxide and SiNTs/iron oxide NPs systems are investigated with respect to the $Fe_3O_4$ particle size. First the magnetization dependence on the applied magnetic field is investigated, and second temperature dependent magnetization measurements have been performed to determine the transition between superparamagnetic behavior and blocked state of the systems, at the so called blocking temperature $T_B$. Magnetic characterization of porous silicon with infiltrated iron oxide NPs of different sizes (4, 5, and 8 nm) has been carried out previously.[24,25] Since the microstructure of the porous silicon and SiNTs differs significantly, a measureable difference for the magnetic coupling of $Fe_3O_4$ NPs housed within porous silicon and between the same NPs confined within the SiNTs is anticipated.

Magnetization measurements have been carried out with a Vibrating Sample Magnetometer (VSM) in the field range between ±1 T and temperatures between 4 and 300 K. The temperature dependent magnetization measurements show a blocking temperature which strongly depends on the particle size but also on the distance between neighboring particles filled within the pores/tubes. The particle–particle distance of the iron oxide NPs within a given pore/tube is on average equal in both cases, and for closest packed environments, a minimum of twice the thickness of the organic coating (4 nm) that is equivalent for all of the NPs studied here. Therefore magnetic exchange coupling is excluded but magnetization

 

measurements show that $Fe_3O_4$ NPs with a size greater or equal to 8 nm infiltrated in pSi dipolarly couple (due to their greater magnetic moment), whereas small NPs (4 and 5 nm) do not couple. In the case of the smaller particles, the surface-to-volume ratio is enhanced which results in an increase of the spin disorder at the particle surface. For smaller nanoparticles the saturation magnetization decreases due to these increasing surface spin-disorder effects.[26] The bigger particles, 8 and 10 nm, magnetically interact, which increases $T_B$ above the value of isolated particles.

To a first approximation, the thermal energy associated with this system can be expressed as:

$$25k_BT_B = K_1V\left(1 - \frac{\mu_0 M_S H_C}{2K_1}\right)^2$$

here $K$ refers to the anisotropy constant, $M_S$ the saturation magnetization, $H_C$ the coercive field, and $V$ the volume of an individual particle. In using this relation for isolated 8 nm particles an estimated value of $T_B$ of 10 K, and for 10 nm particles of 20 K is obtained, if the anisotropy constant $K_1$ of bulk $Fe_3O_4$ is used ($K_1 = 1.35 \times 10^4$ J m$^{-3}$).[27] Nevertheless one has to be aware that the anisotropy constant of a single particle changes with the reduction of its size, and also magnetic inter-particle interactions lead to an enhancement of the magnetic anisotropy of the system.[28] Using the experimental measured values of $T_B$ for the four iron oxide particle sizes, 4, 5, 8 and 10 nm infiltrated within SiNTs (assuming that they do not interact), one can estimate $K_1$ values as follows: for 10 nm particles ($T_B$ = 30 K) $K_1 = 1.98 \times 10^4$ J m$^{-3}$, 8 nm particles ($T_B$ = 20 K) $K_1 = 2.5 \times 10^4$ J m$^{-3}$, 5 nm particles ($T_B$ = 15 K) $K_1 = 7.9 \times 10^4$ J m$^{-3}$ and for 4 nm particles ($T_B$ = 12 K) $K_1 = 1.2 \times 10^5$ J m$^{-3}$. These values deviate from the bulk-value and they are also higher than those reported by Luo *et al.* which deals with a frozen ferrofluid,[29] where magnetic interactions can be neglected. Likely reasons for this deviation include (1) weak magnetic coupling or (2) surface effects associated with the oleic acid coating of the particles. Considering the two nanocomposite systems, one can say that the estimated values of the anisotropy constants well represent the SiNT/$Fe_3O_4$ system, but not in the case of the pSi matrix where strong dipolar coupling takes place when bigger $Fe_3O_4$ particles are present. This data is also summarized in Table 1. Fig. 4 shows a comparison of the temperature dependent magnetization between pSi and SiNTs filled with iron oxide NPs in the case of all different particle sizes measured here.

**Table 1** Size dependent blocking temperatures of porous silicon (pSi) and SiNTs filled with $Fe_3O_4$ NPs. The wall-thickness of the SiNTs is 70 nm

| NP size (nm) | pSi $T_B$ (K) | SiNTs $T_B$ (K) |
|---|---|---|
| 4 | 12 | 12 |
| 5 | 15 | 15 |
| 8 | 160 | 20 |
| 10 | 170 | 40 |

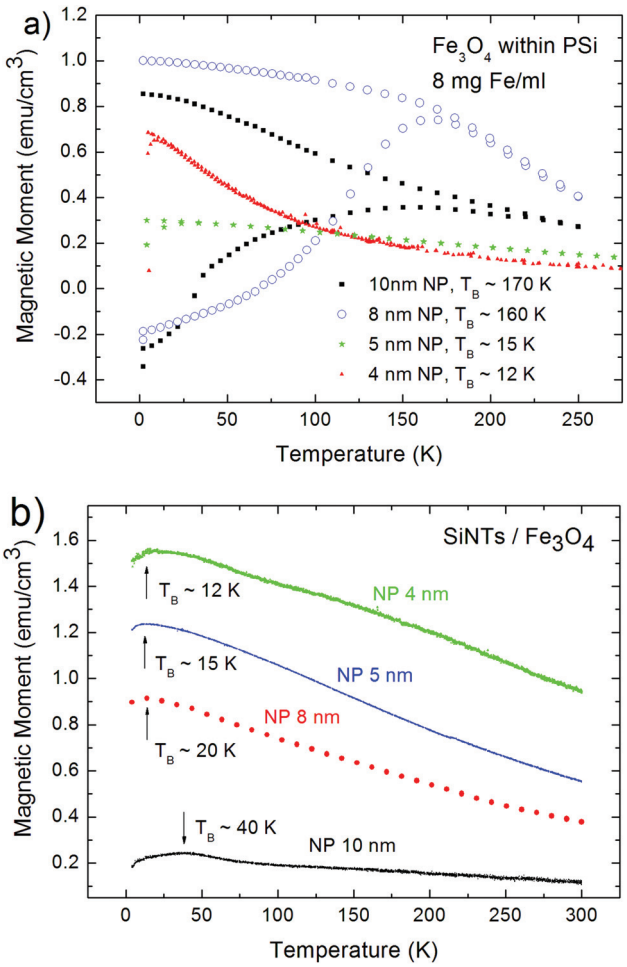


**Fig. 4** ZFC/FC measurements showing the comparison between PSi and SiNTs filled with iron oxide NPs of 4, 5, 8 and 10 nm in size: (a) shift of $T_B$ from 10 K (4 nm) to 170 K (10 nm) of porous silicon samples filled with iron oxide NPs; (b) size dependent shift of $T_B$ in the case of SiNTs filled with $Fe_3O_4$-NPs.

In both nanostructured Si hosts, the observed $T_B$ values for the 4 nm and 5 nm $Fe_3O_4$ NPs are the same. In moving to the larger 8 nm and 10 nm NPs, there are radical differences in the $T_B$ values between SiNTs and pSi, as the pSi templates have relative large values of 160 and 170 K, respectively, while the SiNT system with 70 nm wall thickness demonstrated suppressed $T_B$ values of 20 and 40 K for the infiltrated 8 and 10 nm iron oxide nanoparticles, respectively. A comparison of these experimentally-obtained values with the theoretical ones of isolated nanoparticles shows that in the case of pSi with infiltrated 8 and 10 nm NPs strong dipolar interaction between the particles determines the magnetic properties, whereas in the case of SiNTs inter-particle interactions are suppressed.

As the intrapore $Fe_3O_4$ NP separation distance of 4 nm between the closely packed particles in both types of samples is comparable, the reason for the rather pointed differences between evolution of $T_B$ values as a function of iron oxide particle size between the two porous matrices is likely due to the

different morphologies of the two systems. It is possible that some contributions from surface chemistry are present (*e.g.* different interactions between a given NP and the pore-wall/tube-wall, leading to different surface contributions to the magnetization), but the dominant oxide termination in each type of Si matrix leads to the conclusion that such effects are expected to be subtle.

An increase of the blocking temperature is caused by dipolar coupling between the particles. Given the rather significant differences in pore geometry between the two silicon materials, the suppression of coupling in the case of SiNTs is ascribed to be morphological in origin. Recall that in both Si templates, the dominant surface chemistry is oxide. In the SiNT case, the rather thick oxide separation (2 × 70 nm = 140 nm) for the data shown provides an effective barrier to long range coupling and the observed evolution in blocking temperature a function of $Fe_3O_4$ particle size. For pSi, magnetic coupling makes an appearance at the 8 nm iron oxide threshold, due to the dendritic microstructure of the porous silicon and associated roughness of the walls of the pSi which reduces the mean interpore distance to values of about 20 nm. Thus there is clearly a smaller physical separation in the case of pSi templates.

Furthermore, a commercial 10 nm $Fe_3O_4$ nanoparticle solution (Aldrich) with a rather broad size distribution (ESI†) has been used for the infiltration into SiNTs. In this case three distinct peaks (Fig. 5) have been observed in the temperature dependent magnetization curve.

This detection of multiple blocking temperatures mirrors the observed size distribution, consisting mainly of 10 nm ($T_B$ ~ 30 K), 17.5 nm ($T_B$ ~ 110 K) and 20 nm ($T_B$ ~ 160 K) NPs.

These particle sizes have been estimated by taking the anisotropy constant of bulk magnetite, the measured blocking temperatures and assuming that the particles do not interact.

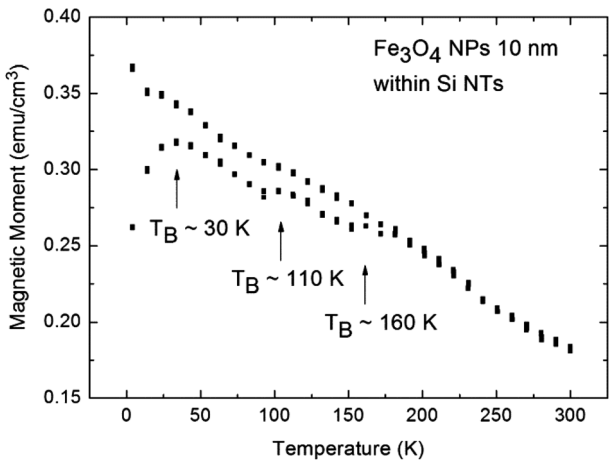


**Fig. 5** ZFC/FC measurements showing the effect of infiltrating a 10 nm $Fe_3O_4$ NP sample with a polydisperse size range into a SiNT template with a 70 nm wall thickness. Three distinct peaks of $T_B$ appear due to this particle solution containing different particle sizes indicating that the particles do not magnetically interact.

The latter assumption is also indicated by the separation of the three peaks. In the case of magnetic interactions one broad peak would appear in the temperature dependent magnetization curve. So in the case of the SiNTs filled with iron oxide NPs possessing this type of polydisperse size distribution, it is possible to distinguish between particle sizes in a "filling solution" due to their non-interacting or very weak interacting behavior. The deviation of the $T_B$-peak between the 10 nm $Fe_3O_4$ NP solution ($T_B$ ~ 40 K) and the commercial 10 nm iron oxide solution ($T_B$ ~ 30 K) arises because the two kinds of particles are slightly different in their size.

Additional magnetic measurements were obtained on SiNTs of 10 nm wall thickness and loaded with the same $Fe_3O_4$ NPs (4, 5, 8, and 10 nm average diameter). The blocking temperature is found to be relatively insensitive to a variation of the wall-thickness of the SiNTs (ESI Table 1†). For a given $Fe_3O_4$ NP size evaluated, reduction of the SiNT wall-thickness to 10 nm results in a change of $T_B$ within a range of only 5 degrees or less.

Considering the hysteresis curves of the Si NTs samples, one can conclude that the coercivity decreases with decreasing particle size, measured at $T$ = 4 K, when the nanocomposite is in the blocked state. In the case of 10 nm $Fe_3O_4$ NPs loaded into SiNTs, $H_C$ is between 600 and 500 Oe and it decreases to 360 Oe for 8 nm $Fe_3O_4$ NPs and further to 200 Oe for 5 nm and 4 nm $Fe_3O_4$ NPs. In the case of pSi loaded with $Fe_3O_4$ NPs the coercivities for 10 and 8 nm $Fe_3O_4$ particles is in the range of 1500 Oe and for the smaller NPs (5 and 4 nm) around 300 Oe. Particles of the sizes used here offer a single domain behavior, whereas the coercivity for a given temperature below $T_B$ (blocked state) decreases with decreasing particle size due to the superparamagnetic relaxation effects.[30]

The SiNT/$Fe_3O_4$ composite is an interesting system with respect to its magnetic behaviour, with the possibility to estimate not only the particle size but also the anisotropy constant of the infiltrated nanoparticles (since their magnetic coupling is negligible). This method enables, on the one hand, a means to cross-check existing TEM images and on the other hand, the possible characterization of the system without the need for additional microscopy. Furthermore, these composite systems are appropriate for possible applicability in biomedicine due to their biocompatibility and the superparamagnetic behaviour. One option in this regard could be in the area of magnetic field-guided drug delivery. In this case the superparamagnetic behaviour of the system is necessary to inhibit particle agglomeration in the circulatory system.

All samples offer a negligible coercivity at $T$ = 300 K being far above $T_B$, which means that no magnetic remanence is present and thus the magnetization of the samples vanishes if the applied magnetic field is switched off. Both biocompatibility and negligible magnetic remanence are of importance for ultimately utilizing the system in an application such as magnetically guided drug delivery. One advantage of the nanocomposites presented here is the possibility to increase the maximum magnetization with the amount of loading of the nanoparticles within the nanostructured silicon vehicle to

 

facilitate its movement within body fluids with simultaneous negligible remanence (without an applied magnetic field). In addition to citation of the known bioactivity/biocompatibility of pSi cited above, the biocompatibility of $Fe_3O_4$ nanoparticles has also been shown by various authors[31,32] and the cytocompatbility of SiNTs with different wall thickness has been evaluated.[33]

## Conclusions

In summary, we investigated the temperature dependent magnetic properties of different iron oxide loaded nanostructured silicon nanocomposites, namely consisting of porous silicon and silicon nanotubes, respectively. Iron oxide nanoparticles of 4, 5, 8 and 10 nm have been encapsulated in these matrices. In this work, the sensitive role of Si host matrix morphology on fundamental magnetic properties of loaded $Fe_3O_4$ has been demonstrated, with the SiNT arrays providing clear suppression of magnetic coupling, even with the largest iron oxide nanoparticle sizes examined (10 nm). However, it is also important to emphasize that even for the case of pSi structures filled with 8 or 10 nm superparamagnetic nanoparticles in a closely packed way, $T_B$ is still far below room temperature and the magnetic preconditions for bioapplications are still fulfilled. The advantage is that the magnetic moment of the system is enhanced compared to smaller particles. The magnetic moment could be increased from 9.3 emu $cm^{-3}$ to 22.2 emu $cm^{-3}$ by utilizing 8 nm $Fe_3O_4$-NPs instead of 5 nm NPs. However, for iron oxide nanoparticles loaded into either matrix (pSi or SiNTs) a negligible magnetic remanence at room temperature is found, an overall promising result for utilizing this system in magnetic field-guided drug delivery. The movement of the porous silicon/$Fe_3O_4$ as well as of the SiNTs/$Fe_3O_4$ composites can be easily carried out in an aqueous solution in a petri dish by applying a magnetic field of 0.1 T.

## Acknowledgements

The authors thank Dr Puerto Morales from the Institute of Material Science, CSIC Madrid, Spain for supplying iron oxide nanoparticles, Dr Peter Pölt from the Institute for Electron Microscopy, University of Technology Graz, Austria for SEM images of iron oxide filled porous silicon and Dr Mihaela Albu also from the Institute for Electron Microscopy, University of Technology Graz, Austria for TEM images of porous silicon. Financial support by the Robert A. Welch Foundation (JLC, Grant P-1212) and the TCU Initiative for Oncology Research (Moncrief Foundation, to JLC) is gratefully acknowledged.

## References

1 P. Apiratikul, A. M. Rossi and Th. E. Murphy, *Opt. Express*, 2009, **17**, 3396.
2 C. Baker and J. L. Gole, *JSM Nanotechnol. Nanomed.*, 2014, **2**, 1021.
3 Y. Mirsky, A. Nahor, E. Edrei, N. Massad-Ivanir, L. M. Bonanno, E. Segal and A. Sa'ar, *Appl. Phys. Lett.*, 2013, **103**, 033702.
4 H. A. Santos, *Porous silicon for biomedical applications*, Woodhead Publishing, 2014.
5 J. M. Buriak, *Philos Trans. R. Soc. London, Ser. A*, 2006, **364**, 2017.
6 H. Föll, M. Christophersen, J. Carstensen and G. Hasse, *Mater. Sci. Eng.*, 2002, **R39**, 93–141.
7 E. Pastor, E. Matveeva, V. Parkhutik, J. Curiel-Esparza and M. C. Millan, *Phys. Status Solidi C*, 2007, **4**, 2136–2140.
8 K. Fukami, K. Kobayashi, T. Matsumoto, Y. L. Kawamura, T. Sakka and Y. H. Ogata, *J. Electrochem. Soc.*, 2008, **155**, D443.
9 C. Pacholski, M. Sartor, M. J. Sailor, F. Cunin and G. M. Miskelly, *J. Am. Chem. Soc.*, 2005, **127**, 11636.
10 L. T. Canham, *Adv. Mater.*, 1995, **7**, 1033.
11 J. Xie, J. Huang, X. Li, S. Sun and X. Chen, *Curr. Med. Chem.*, 2009, **16**, 1278.
12 C. Martinez-Boubeta, K. Simeonidis, A. Makridis, M. Angelakeris, O. Iglesias, P. Guardia, A. Cabot, L. Yedra, S. Estrade, F. Peiro, Z. Saghi, P. A. Midgley, I. Conde-Leboran, D. Serantes and D. Baldomir, *Sci. Rep.*, 2013, **3**, 1652.
13 R. Thomas, I. K. Park and Y. Y. Jeong, *Int. J. Mol. Sci.*, 2013, **14**, 15910.
14 S. C. McBain, H. H. P. Yiu and J. Dobson, *Int. J. Nanomed.*, 2008, **3**, 169.
15 S. Laurent, D. Forge, M. Port, A. Roch, C. Robic, L. Vander Elst and R. N. Muller, *Chem. Rev.*, 2008, **108**, 2064–2110.
16 D. Fine, A. Grattoni, R. Goodall, S. S. Barsal, C. Chiappini, S. Hosali, A. L. van de Ven, S. Srinivasan, X. Liu, B. Godin, L. Brousseau, I. K. Yazdi, J. Fernandez-Moure, E. Tasciotti, H. J. Wu, Y. Hu, S. Klemm and M. Ferrari, *Adv. Healthcare Mater.*, 2013, **2**, 632.
17 L. Russo, F. Colangelo, R. Cioffi, I. Rea and L. De Stefano, *Materials*, 2011, **4**, 1023.
18 X. Huang, R. Gonzalez-Rodriguez, R. Rich, Z. Gryczynski and J. L. Coffer, *Chem. Commun.*, 2013, **49**, 5760.
19 E. Tasciotti, X. Liu, R. Bhavane, K. Plant, A. D. Leonard, B. K. Price, M. M. C. Cheng, P. Decuzzi, J. M. Tour, F. Robertson and M. Ferrari, *Nat. Nanotechnol.*, 2008, **3**, 151.
20 C. A. Poland, R. Duffin, I. Kinloch, A. Maynard, W. A. H. Wallace, A. Seaton, V. Stone, S. Brown, W. MacNee and K. Donaldson, *Nat. Nanotechnol.*, 2008, **3**, 423.
21 S. Sun and H. J. Zeng, *Am. Chem. Soc.*, 2002, **124**, 8204.
22 A. G. Roca, M. P. Morales, K. O'Grady and C. J. Serna, *Nanotechnology*, 2006, **17**, 2783.
23 P. Granitzer and K. Rumpf, *Materials*, 2010, **3**, 943.
24 K. Rumpf, P. Granitzer, P. Morales, P. Pölt and M. Reissner, *Nanoscale Res. Lett.*, 2012, **7**, 445.

25 P. Granitzer, K. Rumpf, M. Venkatesan, A. G. Roca, L. Cabrera, M. P. Morales, P. Poelt and M. Albu, *J. Electrochem. Soc.*, 2010, **157**, K145.
26 J. M. D. Coey, *Phys. Rev. Lett.*, 1971, **27**, 1140.
27 J. Mazo-Zuluaga, J. Restrepo and J. Mejia-Lopez, *Phy. Rev. B: Condens. Matter*, 2007, **398**, 187.
28 A. Espinosa, A. Munoz-Noval, M. Garcia-Hernandez, A. Serrano, J. Jimenez de la Morena, A. Figuerola, A. Quarta, T. Pellegrino, C. Wilhelm and M. A. Garcia, *J. Nanopart. Res.*, 2013, **15**, 1514.
29 W. Luo, S. R. Nagel, T. F. Rosenbaum and R. E. Rosensweig, *Phys. Rev. Lett.*, 1991, **67**, 2721.
30 G. F. Goya, T. S. Berquo, F. C. Fonseca and M. P. Morales, *J. Appl. Phys.*, 2003, **94**, 3520.
31 B. Ankamwar, T. C. Lai, J. H. Huang, R. S. Liu, M. Hsiao, C. H. Chen and Y. K. Hwu, *Nanotechnology*, 2010, **21**, 075102.
32 V. Zavisova, M. Koneracka, J. Kovac, M. Kubovcikova, I. Antal, P. kopcansky, M. Bednarikova and M. Muckova, *J. Magn. Magn. Mater.*, 2015, **380**, 85.
33 Y. Tian, R. Gonzalez, G. R. Akkaraju and J. L. Coffer, Silicon Nanotube-Based Gene Delivery, 9$^{Th}$ International Porous Semiconductors – Science and Technology Conference, 2014, Extended Abstract 240.

 